

# Weighted Approximate Quantum Natural Gradient for Variational Quantum Eigensolver

Chenyu Shi,<sup>1,2,\*</sup> Vedran Dunjko,<sup>1,2,†</sup> and Hao Wang<sup>1,2,‡</sup>

<sup>1</sup>*{aQa<sup>L</sup>} Applied Quantum Algorithms, Universiteit Leiden*

<sup>2</sup>*LIACS, Universiteit Leiden, Niels Bohrweg 1, 2333 CA Leiden, Netherlands*

Variational quantum eigensolver (VQE) is one of the most prominent algorithms using near-term quantum devices, designed to find the ground state of a Hamiltonian. In VQE, a classical optimizer iteratively updates the parameters in the quantum circuit. Among various optimization methods, quantum natural gradient descent (QNG) stands out as a promising optimization approach for VQE. However, standard QNG only leverages the quantum Fisher information of the entire system and treats each subsystem equally in the optimization process, without accounting for the different weights and contributions of each subsystem corresponding to each observable. To address this limitation, we propose a Weighted Approximate Quantum Natural Gradient (WA-QNG) method tailored for  $k$ -local Hamiltonians. In this paper, we theoretically analyze the potential advantages of WA-QNG compared to QNG from three distinct perspectives and reveal its connection with the Gauss-Newton method. We also show it outperforms standard quantum natural gradient descent in the numerical experiments for seeking the ground state of the Hamiltonian.

## I. INTRODUCTION

Quantum computing is widely regarded as having potential advances in numerous fields. However, due to the limitations of the noise and scale of current Noisy Intermediate-Scale (NISQ) quantum devices [1], algorithms such as Shor's [2] and Grover's [3] still remain beyond practical implementation. A computational paradigm well-suited for current NISQ quantum devices is that of the variational quantum algorithms, which is a kind of variational hybrid approach [4]. These algorithms leverage a feedback loop between classical and quantum computers. In this paradigm, the quantum computer evaluates an objective function formulated by a parameterized quantum circuit, while the classical computer employs an optimizer to iteratively update the circuit parameters to seek the optimal value [5].

Variational quantum algorithms have drawn significant attention across various fields, including quantum physics and quantum chemistry [6, 7], optimization [8, 9], and machine learning [10, 11]. Among these, one of the most well-known variational quantum algorithms is the Variational Quantum Eigensolver (VQE) [7]. VQE is designed to find the ground state of a given quantum system. In this algorithm, a variational quantum circuit is employed to estimate the expectation value of the system with respect to a given Hamiltonian. Additionally, a classical optimizer iteratively updates the parameters in the quantum circuit to minimize the expectation value. Through this optimization process, the algorithm is expected to converge to a solution that closely approximates the ground state.

The optimizer in VQE plays a crucial role in deter-

mining the algorithm's performance. In addition to the most basic gradient descent method (referred to as vanilla gradient descent in this context), more advanced variants such as stochastic gradient descent (SGD) [12] and Adam [13] are widely adopted. Among these, quantum natural gradient descent (QNG) [14] emerges as a promising approach. It is the quantum analog of natural gradient descent [15, 16] in its classical counterpart. QNG leverages the quantum Fisher information matrix [17] of the quantum system. It captures the geometric information and is expected to obtain better convergence performance in the optimization process.

In the standard formulation of QNG, the quantum Fisher information used in the optimization step corresponds to the entire quantum system. However, in VQE, particularly in quantum chemistry, the Hamiltonian  $H$  is often expressed as a summation of several  $k$ -local observables, where  $H = \sum_m h_m H_m$  with the corresponding output of the quantum circuit  $\text{tr}(\rho H) = \sum_m h_m \text{tr}(\rho_m H_m)$ . Consequently, each subsystem  $\rho_m$  corresponding to each  $k$ -local observable  $H_m$  contributes differently to the final output of the quantum circuit due to the different weights  $h_m$ . Therefore, a potential improvement for standard QNG is to also assign these subsystems with different weights during the training, rather than only using the quantum Fisher information matrix of the entire system, where all subsystems are treated equally.

Here we propose a new approach, the Weighted Approximate Quantum Natural Gradient Descent (WA-QNG), which takes the different weights and contributions of the subsystem corresponding to each  $k$ -local observable term into account. In WA-QNG, we replace the quantum Fisher information matrix of the entire quantum system with the weighted summation of the Hilbert-Schmidt metric tensors of the subsystems corresponding to each observable in the optimization step. We theoretically analyze the potential advantages of WA-QNG compared to QNG from three distinct perspectives and

\* c.shi@liacs.leidenuniv.nl

† v.dunjko@liacs.leidenuniv.nl

‡ h.wang@liacs.leidenuniv.nl

reveal its connection to the Gauss-Newton method. Our method displays efficient convergence speed compared to standard QNG in the numerical experiments. Furthermore, we show that the Hilbert-Schmidt metric tensor required for WA-QNG can be efficiently estimated using the classical shadow method [18] for  $k$ -local Hamiltonians.

The remainder of the paper will be structured as follows. Section II introduces the preliminary background knowledge, including the variational quantum eigensolver and quantum natural gradient descent. Section III formulates the WA-QNG method and theoretically analyzes its potential advantages over standard QNG from three different perspectives. Section IV explores the connection between WA-QNG and the Gauss-Newton method. Section V presents the numerical experimental results to support our theoretical analysis. Finally, Section VI concludes the paper.

## II. BACKGROUND

In this section, we provide a brief overview of the foundational background relevant to this paper. First, we briefly introduce VQE and explain its working principles. Then, we give the definition of quantum natural gradient descent and discuss its relation with quantum Fisher information.

### A. Variational Quantum Eigensolver

The goal of the VQE, initially introduced by [7], is to approximately seek the ground state  $\rho_{GS}$  with respect to a Hamiltonian  $H$ . A variational quantum circuit is used to prepare a variational quantum state  $\rho_\theta$ , where  $\rho_\theta = U(\theta)|0\rangle\langle 0|U^\dagger(\theta)$ . The expectation value with respect to the Hamiltonian  $H$  is evaluated by the quantum computer. An illustration of variational quantum circuit in VQE is given in Fig. 1. Hence, the variational quantum circuit realizes the following function  $f$ :

$$f(\theta) = \text{tr}(\rho_\theta H) \quad (1)$$

According to the definition, the ground state  $\rho_{GS}$  is the lowest energy state of the given Hamiltonian  $H$ . Hence, seeking the ground state by adjusting the parameter  $\theta$  is equivalent to minimizing the function  $f(\theta)$ .

The value of function  $f(\theta)$  is fed to a classical computer in the optimization process. The classical computer employs an optimizer, where  $f(\theta)$  is the objective function, to iteratively update the parameters in the quantum circuit. The most common optimization method is the vanilla gradient descent. In each optimization step, the parameters are updated by:

$$\theta^{(k+1)} = \theta^{(k)} - \eta \nabla f(\theta^{(k)}) \quad (2)$$

where  $\nabla f$  is the gradient of the objective function and  $\eta$  is the learning rate. In general, the gradient can be

approximated using a naive finite difference method. In VQE, however, the most common approach to obtain the exact gradient is through the parameter-shift rule [19, 20], up to finite sampling errors.

The general working principle of VQE is also illustrated in Fig. 1. After sufficient training with an expressive variational circuit, VQE is expected to produce a good approximation of the ground state.

### B. Quantum Natural Gradient Descent

Each optimization update step in vanilla gradient descent can be formulated as the following constrained optimization problem [16, 21] for a small  $\varepsilon$  with a small change  $\delta$  in parameter space:

$$\begin{aligned} \min_{\delta} \quad & f(\theta + \delta) \\ \text{s.t.} \quad & \|\delta\|_2^2 \leq \varepsilon \end{aligned} \quad (3)$$

This constrained optimization problem seeks to minimize the objective function  $f$  within a local neighborhood of  $\theta^{(k)}$ . Note that solving this problem by applying a first-order Taylor approximation to  $f$  leads to the derivation of the vanilla gradient descent step in Eq. (2).

A limitation of this method is that each step is inherently tied to the Euclidean geometry of the parameter space, as the Euclidean distance is used to define the local neighborhood in the constrained optimization problem. However, the distances in the optimization landscape can be distorted in reparameterization – for example, directions that were equally steep may become scaled differently, potentially leading to inefficiencies in the optimization process [14, 15].

An illustration is shown in Fig. 2. The parameter space is a Euclidean space  $[0, \pi] \times [0, 2\pi]$ , where each coordinate corresponds to the polar angle and azimuthal angle of a sphere. The parametrization maps each point in the original parameter space to a point on the surface of a unit sphere using the coordinate transformation  $x = \sin(\theta) \cos(\phi)$ ,  $y = \sin(\theta) \sin(\phi)$ ,  $z = \cos(\theta)$ . In the original parameter space, the distances between points  $A$  and  $B$  (red line) and between points  $C$  and  $D$  (purple line) are the same in terms of Euclidean distance. However, after parametrization onto the sphere, their distances differ significantly<sup>1</sup>. An intuitive example is as follows: Suppose the original parameter space consists of latitude and longitude pairs, and the parametrization maps each pair to a point on the surface of the Earth. It is more natural to describe distances using the great-circle path distance

<sup>1</sup> In Fig. 2, we use the chord length as the distance metric between two points on the sphere for simplicity. Note that the chord length is always proportional to the great-circle distance, which represents the true geodesic distance on the sphere.

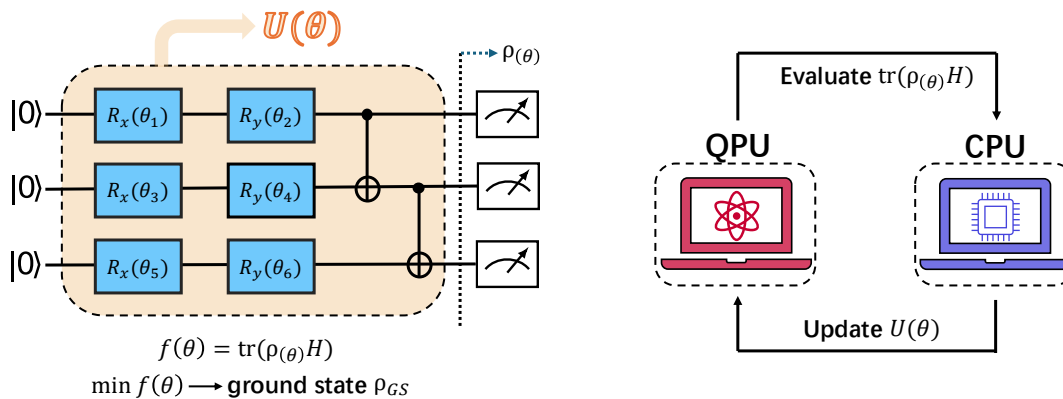


FIG. 1. Left: An illustration of the variational quantum circuit in VQE. A parameterized quantum circuit  $U(\theta)$  is used to prepare a variational quantum state  $\rho_\theta$ . By adjusting the parameter  $\theta$ , the quantum circuit aims to prepare the state  $\rho_\theta$  that approximates the ground state  $\rho_{GS}$  by minimizing the objective function  $f(\theta)$ . Right: The general working principle of VQE. The quantum computer evaluates the expectation value  $f(\theta) = \text{tr}(\rho_\theta H)$ , while the classical computer employs an optimizer to iteratively update the parameters  $\theta$  to minimize the objective function  $f(\theta)$ .

defined directly on the Earth's surface (i.e., distance after parametrization) rather than the Euclidean distance between latitude and longitude pairs (i.e., distance in the parameter space).

Similarly, in the parametrization from the parameter  $\theta$  to the variational quantum state  $\rho_\theta$ , the distance distortion can also occur. Changes with the same Euclidean distance in the parameter space can result in different changes in the variational quantum state  $\rho_\theta$ . Therefore, it is more natural to use a distance metric defined directly for the variational quantum state  $\rho_\theta$  to reformulate the constrained optimization problem, rather than relying on the Euclidean distance defined for  $\theta$  in the original parameter space:

$$\begin{aligned} \min_{\delta} \quad & f(\theta + \delta) \\ \text{s.t.} \quad & D_F(\rho_\theta, \rho_{\theta+\delta}) \leq \varepsilon \end{aligned} \quad (4)$$

where the distance metric  $D_F(\rho, \sigma) = 1 - (\text{tr}(\sqrt{\sqrt{\rho}\sigma\sqrt{\rho}}))^2$  is the fidelity distance. For pure states  $\rho = |\phi\rangle\langle\phi|$  and  $\sigma = |\psi\rangle\langle\psi|$ , the fidelity distance can also be formulated as  $D_F(|\phi\rangle, |\psi\rangle) = 1 - |\langle\phi|\psi\rangle|^2$ . Solving the above optimization problem derives the quantum natural gradient (QNG) update step:

$$\theta^{(k+1)} = \theta^{(k)} - \eta F^+ \nabla f(\theta^{(k)}) \quad (5)$$

where  $F^+$  is the pseudo-inverse of the quantum Fisher information matrix  $F$  at  $\theta^{(k)}$ , and  $\eta$  is the learning rate. For a pure state  $|\psi(\theta)\rangle$ , the quantum Fisher information matrix  $F$  is given by:

$$F_{ij} = 4 \text{Re} \left\{ \left\langle \frac{\partial\psi}{\partial\theta_i} \middle| \frac{\partial\psi}{\partial\theta_j} \right\rangle - \left\langle \frac{\partial\psi}{\partial\theta_i} \middle| \psi \right\rangle \left\langle \psi \middle| \frac{\partial\psi}{\partial\theta_j} \right\rangle \right\} \quad (6)$$

where  $\theta_i$  denotes the  $i$ -th element of the parameter  $\theta$ , and  $F_{ij}$  represents the  $(i, j)$ -th entry of the quantum

Fisher information matrix  $F$ . For details on the derivation, please refer to [14] and [22]. A detailed discussion of the derivation is also provided in Appendix D. QNG has been shown to achieve better performance compared to vanilla gradient descent in previous studies [14, 15, 23].

### III. WA-QNG: WEIGHTED APPROXIMATE QUANTUM NATURAL GRADIENT DESCENT

In this section, we present the formulation of the Weighted Approximate Quantum Natural Gradient Descent (WA-QNG) method and discuss its potential advantages. First, we highlight the limitation of QNG, where the weights of subsystems corresponding to each observable are not considered. To address this issue, we introduce WA-QNG, which leverages the weighted sum of the Hilbert-Schmidt metric tensors of each subsystem in the optimization step. Additionally, we demonstrate WA-QNG's potential advantages from three different perspectives.

#### A. Limitation of QNG

The quantum Fisher information matrix of  $\rho_\theta$  in Eq. (5) represents the quantum Fisher information matrix of the entire quantum system. A key limitation is that this quantum Fisher information does not incorporate any information about the Hamiltonian. Consequently, QNG utilizes the same quantum Fisher information matrix  $F$  in the update formula for two different observables. However, in VQE, we care more about how parameter changes affect the final objective function energy value rather than the density matrix itself. Therefore, information about the Hamiltonian should also be taken into account during the optimization process.

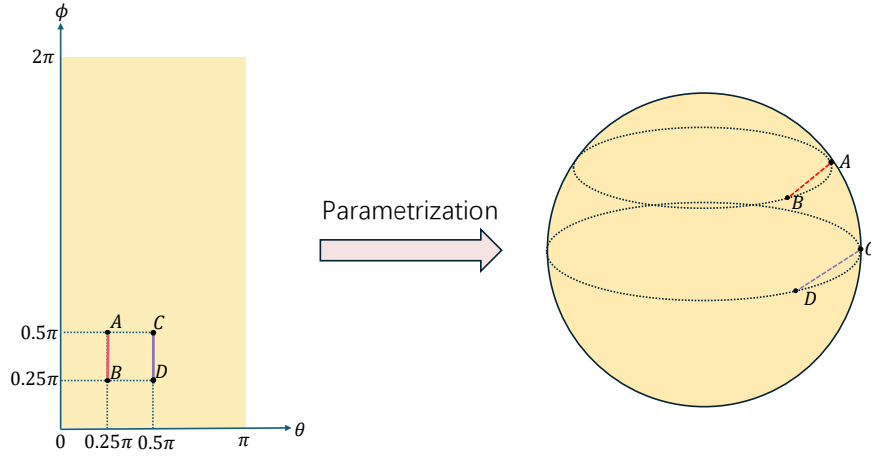


FIG. 2. An illustration of distance distortion in the parametrization. The original parameter space is an Euclidean space. The parametrization maps the point in the parameter space to a point on the sphere with radius  $r = 1$  by the coordinate transformation  $x = \sin(\theta) \cos(\phi)$ ,  $y = \sin(\theta) \sin(\phi)$ ,  $z = \cos(\theta)$ . The distances from  $A$  to  $B$  (red line) and from  $C$  to  $D$  (purple line) are the same in the original parameter space. However, after parametrization to the sphere, the distances are distorted and become different.

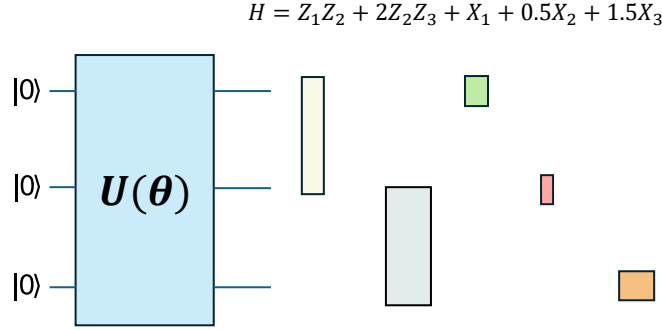


FIG. 3. An illustration when the Hamiltonian is  $H = Z_1 Z_2 + 2Z_2 Z_3 + X_1 + 0.5X_2 + 1.5X_3$ . The small rectangles indicate that the corresponding Hamiltonian term acts on that subsystem. And the width of rectangles reflects the magnitude of each coefficient  $h_m$ . Each subsystem contributes differently to the output due to the coefficients, suggesting that they should be assigned different weights in the optimization process.

Consider a  $k$ -local Hamiltonian  $H = \sum_m h_m H_m$  and its expectation value  $\text{tr}(\rho_\theta H) = \sum_m h_m \text{tr}(\rho_m H_m)$ , where each  $H_m$  is a Pauli string that acts non-trivially on a subsystem state  $\rho_m$  of  $k$  qubits. Intuitively, the contributions of each subsystem  $\rho_m$  are different due to the associated weights  $h_m$ . An illustration (shown in Fig. 3) is the 3-qubit toy Hamiltonian  $H = Z_1 Z_2 + 2Z_2 Z_3 + X_1 + 0.5X_2 + 1.5X_3$ . The contributions of the five subsystems, corresponding to the five terms in the Hamiltonian, are weighted by their respective coefficients. Therefore, in the optimization process, a potential improvement is to also assign appropriate weights to each subsystem, rather than treating them equally as in standard QNG. In addition, as the total system size increases, the parameter sensitivity within each subsystem may differ significantly from that of the entire system. In such cases, the quantum Fisher information matrix  $F$  of the entire system may struggle to capture the parameter sensitivity of

each subsystem. To address all these aspects that are overlooked in QNG, we propose the WA-QNG method.

## B. Method Formulation

In this subsection, we formalize the WA-QNG method. Suppose the target Hamiltonian to solve is  $H = \sum_m h_m H_m$ . Then the update formula of WA-QNG is then given by:

$$\theta^{(k+1)} = \theta^{(k)} - \eta W^+ \nabla f(\theta^{(k)}) \quad (7)$$

where  $W = \frac{2}{\sum_m h_m^2} \sum_m h_m^2 T_m$ , and  $T_m$  represents the Hilbert-Schmidt metric tensor [24, 25] of the  $m$ -th subsystem corresponding to the observable  $H_m$ . The  $i$ -th row  $j$ -th column element of each  $T_m$  is that  $(T_m)_{ij} =$

$\text{tr}(\partial_i \rho_m \partial_j \rho_m)$ . Because the coefficient  $h_m$  can be negative, we use square-weighted summation instead of direct-weighted summation. The prefactor  $\frac{2}{\sum_m h_m^2}$  is to make WA-QNG consistent with QNG: When each term  $H_m$  in the Hamiltonian non-trivially acts on the whole quantum system, WA-QNG reduces to QNG and  $W = 2T = F$ . The proof of this equivalence is detailed in Appendix A. From this perspective, WA-QNG can be regarded as a more generalized form of the original QNG.

In the following, we further motivate and explain why the matrix  $W$ , namely the weighted average of the Hilbert-Schmidt metric tensors of each subsystem, is chosen in the updated formula of WA-QNG, and also why it is expected to perform well from three different interpretative perspectives. We also show the update formula of WA-QNG can be derived from these three different perspectives. Furthermore, beyond its performance in optimization, we demonstrate in Appendix B that the Hilbert-Schmidt metric tensors  $T_m$  in matrix  $W$  can be efficiently estimated using the classical shadow technique.

### C. Intuitive Interpretation

The quantum Fisher information matrix  $F$  of the entire system is used in the optimization step of QNG. Mathematically, because  $F$  is unrelated to the index  $m$ , it can be rewritten as:

$$\begin{aligned} F &= 1 \cdot F \\ &= \frac{1}{\sum_m h_m^2} \sum_m h_m^2 F \end{aligned} \quad (8)$$

where  $h_m$  is the  $m$ -th coefficient of the  $k$ -local Hamiltonian  $H = \sum_m h_m H_m$ . However, since the  $m$ -th observable  $H_m$  and coefficient  $h_m$  are only associated with the subsystem  $\rho_m$ , an intuitive way to address the different contributions of each subsystem is to replace  $F$  in Eq. (8) with  $F_m$ , the quantum Fisher information matrix of the corresponding subsystem  $\rho_m$ . Therefore, we define a new matrix  $\hat{F}$ :

$$\hat{F} = \frac{1}{\sum_m h_m^2} \sum_m h_m^2 F_m \quad (9)$$

Compared to Eq. (8), Eq. (9) incorporates a weighted sum of the quantum Fisher information matrices of individual subsystems. Here,  $h_m^2$  serves as a weight to quantify the influence of each subsystem. By taking a weighted sum over the quantum Fisher information matrix of each subsystem  $\rho_m$  corresponding to  $H_m$ , this formulation explicitly accounts for the different weights and contributions of each subsystem.

However, since each subsystem state will be a mixed state in general, and as noted in [17, 24, 26], the estimation of the quantum Fisher information for a mixed state is generally a more computationally demanding task than for a pure state. Consequently, estimating the matrix  $F_m$

required in Eq. (9) is computationally demanding. To deal with this problem, references [24, 25] propose using the Hilbert-Schmidt metric tensor  $T$  as an approximation of the quantum Fisher information  $F$  in QNG for a mixed state, where  $F \approx 2T$  when the mixed state is close to being pure and does not change dramatically with parameters. We also demonstrate this approximation relation in Appendix C. Therefore, we can approximate each  $F_m$  in Eq. (9) using the Hilbert-Schmidt metric tensor  $T_m$ :

$$W = \frac{2}{\sum_m h_m^2} \sum_m h_m^2 T_m \quad (10)$$

here we exactly obtain the matrix  $W$  used in Eq. (7) of the update rule of WA-QNG. Eq. (9) introduces a weighted average to account for the relative importance of each subsystem. From Eq. (9) to Eq. (10), the Hilbert-Schmidt metric tensor is employed to approximate the quantum Fisher information matrix of each subsystem state. Hence, this is where the name of our method WA-QNG: *Weighted Approximate Quantum Natural Gradient Descent* comes from.

### D. Optimization Interpretation

The constrained optimization problem defined in Eq. (4) uses the fidelity distance  $D_F$  as the distance metric. As discussed in Section II B, using  $D_F$  instead of the Euclidean distance in the parameter space leads to the derivation of the QNG update formula. However, the distance metric  $D_F$  for the entire quantum system still does not account for the different weights of each subsystem with respect to the observables. To capture this characteristic, we introduce the following distance:

$$D_W(\rho(\theta+\delta), \rho(\theta)) = \frac{2}{\sum_m h_m^2} \sum_m h_m^2 \|\rho_m(\theta+\delta) - \rho_m(\theta)\|_2^2 \quad (11)$$

where  $h_m$  is the  $m$ -th coefficient of the  $k$ -local Hamiltonian  $H = \sum_m h_m H_m$ , and  $\rho_m$  represents the subsystem state of  $\rho(\theta)$  corresponding to the  $m$ -th subsystem. Additionally, the coefficient  $h_m^2$  serves as a weight in the weighted averaging process of the 2-norm distance, thereby accounting for the different contributions of each subsystem. Hence, similar to Eq. (4), we define the following constrained optimization problem for each update step:

$$\begin{aligned} \min_{\delta} \quad & f(\theta + \delta) \\ \text{s.t.} \quad & D_W(\rho(\theta), \rho(\theta + \delta)) \leq \varepsilon \end{aligned} \quad (12)$$

From the constrained optimization problem defined above, we can derive the same update rule of WA-QNG as given in Eq. (7). Thus, we establish WA-QNG from the optimization perspective. The detailed derivation from this optimization problem to WA-QNG is provided in Appendix D.

### E. Geometric Interpretation

The interpretation in the previous subsection can be further explained from the perspective of Riemannian geometry. In general, consider a function  $F : \Theta \rightarrow \mathcal{M}$  from the parameter space  $\Theta \subseteq \mathbb{R}^A$  to a Riemannian manifold  $\mathcal{M}$  equipped with a Riemannian metric  $g_{\mathcal{M}}$ . A pullback metric  $^2 g$  on  $\Theta$  is induced by function  $F$ , which is defined as [27]:

$$\begin{aligned} g_{ij} &:= (F^* g_{\mathcal{M}})(d\theta_i, d\theta_j) \\ &= g_{\mathcal{M}}(\partial_i F(\theta), \partial_j F(\theta)) \end{aligned} \quad (13)$$

Then, the Riemannian gradient descent [14, 15, 28] with pullback metric can be defined for  $\mathcal{M}$ :

$$\theta^{(k+1)} = \theta^{(k)} - \eta g(\theta)^+ \nabla f(\theta^{(k)}) \quad (14)$$

Now, consider a quantum state  $\rho(\theta)$  prepared by a parameterized circuit. For QNG, the quantum circuit defines a mapping function  $F : \mathbb{R}^A \rightarrow \mathbb{H}^N$ , where  $\mathbb{H}^N$  represents the  $N \times N$  Hermitian matrix space. In this view, QNG can be considered to work with the pullback metric of the Frobenius inner product  $g_{\mathbb{H}}(\rho, \sigma) = \text{tr}(\rho\sigma)$  defined on Hermitian matrix space:

$$\begin{aligned} g_{ij}(\theta) &= (F^* g_{\mathbb{H}})(d\theta_i, d\theta_j) \\ &= g_{\mathbb{H}}(\partial_i \rho(\theta), \partial_j \rho(\theta)) \\ &= \text{tr}(\partial_i \rho(\theta) \partial_j \rho(\theta)) \end{aligned} \quad (15)$$

which is consistent with the update rule of QNG in Eq. (5), up to a constant factor 2. In WA-QNG, to address the different weights and contributions of each subsystem, we view the mapping function  $F$  as:

$$\theta \xrightarrow{F} q(\theta) = \frac{1}{\sqrt{\sum_m h_m^2}} [h_1 \rho_1(\theta), \dots, h_M \rho_M(\theta)] \quad (16)$$

where the  $q(\theta)$  is a point in the product space  $\mathbb{H}_1 \times \dots \times \mathbb{H}_M$  where each subsystem  $\rho_m \in \mathbb{H}_m$ . This product space is equipped with an inner product  $\langle (\rho_1, \dots, \rho_M), (\sigma_1, \dots, \sigma_M) \rangle = \sum_{m=1}^M \text{tr}(\rho_m \sigma_m)$ . Similarly, the pullback metric can also be obtained as:

$$\begin{aligned} g_{ij}(\theta) &= \langle \partial_i q(\theta), \partial_j q(\theta) \rangle \\ &= \frac{1}{\sum_m h_m^2} \sum_m h_m^2 \text{tr}(\partial_i \rho_m(\theta) \partial_j \rho_m(\theta)) \end{aligned} \quad (17)$$

which is consistent with the update rule of WA-QNG in Eq. (7), also up to a constant factor 2. Compared to QNG, since each subsystem is explicitly represented with its corresponding coefficient in the direct product space, the pullback Riemannian metric tensor is more likely to account for the different weights of each subsystem.

<sup>2</sup> Strictly, only when  $F$  is an immersion, the pullback metric defined in Eq. (13) is guaranteed actually to be a Riemannian metric. However, the pullback metric defined in Eq. (13) is always well-defined and ensures that the update formula in Eq. (14) works in general.

### IV. RELATION WITH GAUSS-NEWTON METHOD

As illustrated in [16], second-order optimization methods that leverage Fisher information can be interpreted as a generalized Gauss-Newton method. Here, we also demonstrate that the objective function Eq. (1) can be approximately transferred into a weighted non-linear least squares problem when each subsystem is close to being pure and does not change significantly with respect to parameters. Under this condition, we prove that WA-QNG is equivalent to the Gauss-Newton method for this non-linear least squares problem.

Let  $\tilde{H}_m = -H_m$  and  $\hat{H}_m = \frac{\tilde{H}_m}{h_m}$  for simplicity in the derivation. Also note that all constant factors, such as  $\frac{1}{\sum_m h_m^2}$ , do not affect the optimization formulation, as they can ultimately be absorbed into the learning rate. For simplicity, we use the symbol  $\Leftrightarrow$  to represent two minimization problems are equivalent up to a constant factor. Starting from the optimization problem in Eq. (1), we can perform the following transformation:

$$\begin{aligned} &\min_{\theta} \text{tr}(\rho(\theta)H) \\ &\Leftrightarrow \min_{\theta} \frac{1}{\sum_m h_m^2} \sum_m \text{tr}(h_m \rho_m(\theta) H_m) \\ &\Leftrightarrow \min_{\theta} \frac{1}{\sum_m h_m^2} \sum_m -\text{tr}(h_m \rho_m(\theta) \tilde{H}_m) \\ &\approx \min_{\theta} \frac{\sum_m (\text{tr}(h_m^2 \rho_m^2(\theta)) - 2\text{tr}(h_m \rho_m(\theta) \tilde{H}_m) + \text{tr}(\tilde{H}_m^2))}{\sum_m h_m^2} \end{aligned} \quad (18)$$

Note that the third transformation is an approximate one, where two additional terms,  $\text{tr}(h_m^2 \rho_m^2)$  and  $\text{tr}(\tilde{H}_m^2)$ , are added into the summation. The latter is a constant so it does not affect the optimization. For the former, we leverage the assumption that each subsystem is close to being pure and does not change significantly with respect to the parameters. Under this condition, the term  $\text{tr}(h_m^2 \rho_m^2)$  remains close to a constant  $h_m^2$ , while the term  $2\text{tr}(h_m \rho_m \tilde{H}_m)$  dominates the gradient in the optimization problem. When  $\rho_m$  is exactly pure, the approximate transformation becomes exact. We then continue the transformation:

$$\begin{aligned} &\min_{\theta} \frac{\sum_m (\text{tr}(h_m^2 \rho_m^2(\theta)) - 2\text{tr}(h_m \rho_m(\theta) \tilde{H}_m) + \text{tr}(\tilde{H}_m^2))}{\sum_m h_m^2} \\ &\Leftrightarrow \min_{\theta} \frac{1}{\sum_m h_m^2} \sum_m \|h_m \rho_m(\theta) - \tilde{H}_m\|_2^2 \\ &\Leftrightarrow \min_{\theta} \frac{1}{\sum_m h_m^2} \sum_m h_m^2 \|\text{vec}(\rho_m(\theta)) - \text{vec}(\hat{H}_m)\|^2 \end{aligned} \quad (19)$$

In the final expression of Eq. (19), we observe that the original problem is transformed into a non-linear least squares problem. The update formula of Gauss-Newton

method [29] for such a non-linear least squares problem with weights is given by:

$$\theta^{(k+1)} = \theta^{(k)} - \eta(J_r^T J_r)^{-1} J_r^T \vec{r}(\theta^{(k)}) \quad (20)$$

$\vec{r}(\theta)$  is often referred to as the residual vector which is defined in Eq. (21) in our case, and  $J_r$  is the Jacobian of the residual with respect to the parameter  $\theta$ .

$$\vec{r}(\theta) = \frac{[h_1(\text{vec}(\rho_1) - \text{vec}(\hat{H}_1)), \dots, h_M(\text{vec}(\rho_M) - \text{vec}(\hat{H}_M))]^T}{\sqrt{\sum_m h_m^2}} \quad (21)$$

Note that, as the objective function is defined by Eq. (19), where  $f(\theta) = \frac{1}{\sum_m h_m^2} \sum_m h_m^2 \|\text{vec}(\rho_m) - \text{vec}(\hat{H}_m)\|^2 = \vec{r}^T \vec{r}$ , Eq. (20) can be rewritten into:

$$\theta^{(k+1)} = \theta^{(k)} - \eta(2J_r^T J_r)^{-1} \nabla f(\theta^{(k)}) \quad (22)$$

One can verify that the matrix  $W$  defined in WA-QNG satisfies the relation:  $W = 2J_r^T J_r$ . Hence, the update rule in Eq. (22) is fully equivalent to the update rule of WA-QNG in Eq. (7). The details of the relationship between the matrix  $W$  and the Gauss-Newton method are provided in Appendix E.

Thus, we have demonstrated that WA-QNG is approximately equivalent to the Gauss-Newton method for a nonlinear least squares problem, under the assumption that each subsystem is close to being pure and does not vary significantly with respect to the parameters. Under this condition, WA-QNG is expected to inherit the favorable properties of the Gauss-Newton method and has the potential to outperform ordinary gradient descent.

## V. NUMERICAL RESULTS

In this section, we present the results of the numerical experiments. First, we compare the overall performance of standard QNG and WA-QNG for the 1D Ising model and Heisenberg model in Section V A. Additionally, to better evaluate whether the design of WA-QNG to capture the different weights of subsystems effectively improves upon standard QNG, we design experiments to examine the effects of subsystem weights and the number of qubits in Section V B and Section V C respectively.

### A. Performance Comparison

To evaluate the performance of WA-QNG, we test it alongside standard QNG on the variational quantum eigensolver for a 1D Ising model and Heisenberg model. Their Hamiltonians are given as follows, respectively:

$$H = \sum_{\langle ij \rangle} Z_i Z_j + \sum_i X_i \quad (23)$$

$$H = \sum_{\langle ij \rangle} (X_i X_j + Y_i Y_j + Z_i Z_j) \quad (24)$$

The variational quantum circuit used in our experiments is the widely used EfficientSU2, illustrated in Fig. 4 for the 4-qubit, single-layer example. In our experiments, we evaluate QNG and WA-QNG for these two Hamiltonians on 10-, 12- and 14-qubit cases. To maintain simplicity for testing, we use only a single layer in the circuit for experiments.

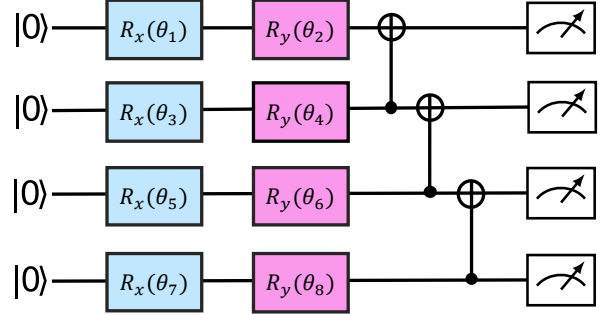


FIG. 4. An example of a 4-qubit EfficientSU2 circuit. It consists of single-qubit rotation gates  $R_x$  and  $R_y$ , followed by a series of CNOT gates to enhance entanglement.

In our experiments, standard QNG is used as the baseline instead of vanilla gradient descent because both QNG and WA-QNG require additional shots to estimate the metric tensor matrix, making a direct comparison with vanilla gradient descent a bit unfair in the same optimization step. For a detailed comparison between QNG and vanilla gradient descent, please refer to [14]. As discussed in Section IV, WA-QNG has a solid theoretical connection between Gauss-Newton method when each subsystem is close to being pure. To achieve this, we propose initializing the variational circuit with small angles to ensure low entanglement at the start. Moreover, small-angle initialization is believed to help mitigate issues such as the Barren Plateau problem [30, 31]. In our experiments, each parameter is uniformly randomly selected from the intervals  $[-0.1, -0.05] \cup [0.05, 0.1]$ . To ensure a fair comparison, the learning rate for both methods is set to 0.02, and the parameters are initialized identically for both methods. Each configuration is independently run ten times, and the learning curves presented in the following sections are averaged over these runs. The experiments are conducted on classical simulators, where both expectation values and the metric tensors can be tracked precisely.

The learning curves of WA-QNG and QNG for the Ising model and Heisenberg model are shown in Fig. 5 and Fig. 6, respectively. WA-QNG exhibits faster optimization convergence speed compared to QNG, indicating that accounting for the different weights of subsystems in WA-QNG effectively improves optimization

performance. Moreover, in the 12- and 14- qubit cases for the Ising model, WA-QNG converges to a lower minimum than QNG, suggesting that WA-QNG may possess a better ability to escape local minima.

### B. Weights of Subsystems

To better understand how accounting for the different weights of each subsystem in WA-QNG plays a central role in improving optimization performance compared to standard QNG, we conduct experiments using the following 3-qubit toy Ising model, with  $\alpha$  set to 0.8, 0.6, 0.4 and 0.2:

$$H = Z_1 Z_2 + Z_2 Z_3 + \alpha X_1 + (3 - 2\alpha)X_2 + \alpha X_3 \quad (25)$$

As  $\alpha$  decreases from 0.8 to 0.2, the weights of the subsystems become increasingly unbalanced, with the contribution of the subsystem associated with the second qubit to the output growing larger. Therefore, if incorporating subsystem weights into the optimization is really effective, WA-QNG is expected to exhibit increasingly better performance compared to QNG as  $\alpha$  decreases.

To intuitively quantify the performance gap between WA-QNG and standard QNG, we use the difference in cost function values at the same optimization step on the learning curves as an indicator. For a fair comparison, this difference is normalized by dividing it by the difference between the initial and converged cost function value. The cost function value gap curve during training and the discrete area under the gap curve (also representing the discrete area between the learning curves of WA-QNG and QNG) are presented in Fig. 7.

As  $\alpha$  decreases from 0.8 to 0.2, the contribution of the subsystem on the second qubit increases. The experimental results align with the theoretical analysis, as the discrete AUC indeed increases with decreasing  $\alpha$ . It indicates that capturing the different weights and contributions of each subsystem in WA-QNG effectively improves optimization performance compared to standard QNG. This result implies that WA-QNG is more suitable for situations where the coefficients of each observable in the  $k$ -local Hamiltonian vary significantly and are unbalanced.

### C. Number of Qubits

As mentioned in Section III A, when the entire system becomes significantly larger than the subsystems that directly contribute to the output, the sensitivity of each parameter in the total system differs considerably from that of each subsystem. Under this condition, WA-QNG is expected to outperform standard QNG to a greater extent. To gain a clearer understanding, we conduct experiments using an  $n$ -qubit toy Ising model Hamiltonian,

with  $n$  varying from 2 to 5:

$$H = \sum_{i=1}^{n-1} Z_i Z_{i+1} + \sum_{i=1}^n X_i \quad (26)$$

As  $n$  increases, the sensitivity of each parameter in each subsystem differs more significantly from that of the entire system, as each observable in  $H$  is at most 2-local. Consequently, WA-QNG is expected to perform increasingly better as  $n$  increases compared to standard QNG. Similar to the previous subsection, the cost function value gap curve during training and the discrete AUC are shown in Fig. 8. For a fair comparison, this difference is also normalized by dividing it by the difference between the initial and converged cost function value.

The experimental results agree with the theoretical analysis. As  $n$  increases, the discrete AUC also increases, indicating a more significant performance improvement for WA-QNG. This suggests that WA-QNG is particularly well-suited for scenarios where the total system size  $n$  is much larger than the locality factor  $k$  for a  $k$ -local Hamiltonian. QNG is a special case of WA-QNG when  $k = n$ .

## VI. DISCUSSION AND CONCLUSION

In this work, we mainly introduce the WA-QNG, which accounts for the different weights and contributions of each subsystem in the optimization process. In particular, we propose using the matrix  $W = \frac{2}{\sum_m h_m^2} \sum_m h_m^2 T_m$  instead of the quantum Fisher information matrix of the entire system in each optimization step. We provide three perspectives to explain the effectiveness and potential advantages of WA-QNG. Firstly, the matrix  $W$  in WA-QNG can be interpreted as an approximation of the weighted average of the quantum Fisher information matrix of each subsystem contributing to the output. Secondly, from an optimization view, we illustrate that WA-QNG can be derived from a constrained optimization problem where the Euclidean distance in the parameter space is replaced by a weighted sum over the 2-norm distances between density matrices. We further explain that WA-QNG can also be derived from an information geometric perspective, where it emerges as a pullback metric. Additionally, we demonstrate that the optimization task can be approximately transformed into a non-linear least squares problem, where WA-QNG is equivalent to the Gauss-Newton method.

To evaluate the performance of WA-QNG, we conduct numerical experiments on the variational eigensolver for the Ising model and Heisenberg model. The results indicate that WA-QNG achieves superior optimization performance compared to standard QNG. Additionally, we perform further experiments to investigate the source of WA-QNG's advantage. Our findings indicate two key factors. The first is accounting for the weights of each sub-



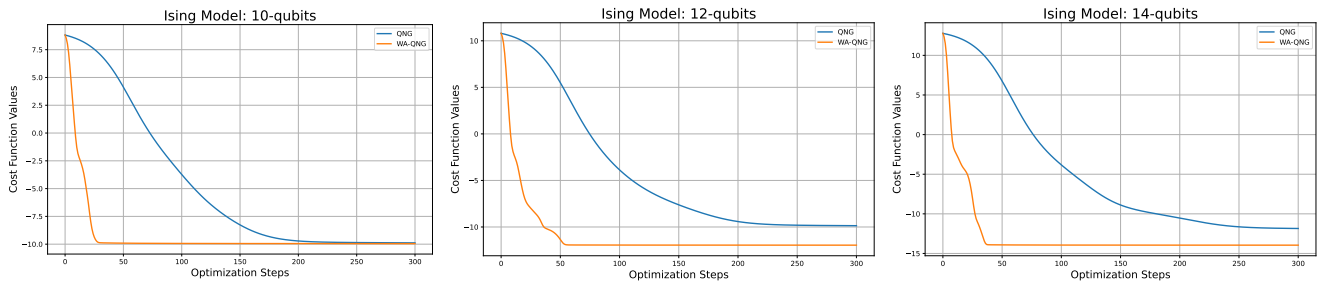


FIG. 5. The learning curves of the two methods for Ising model of 10, 12, 14 qubits.

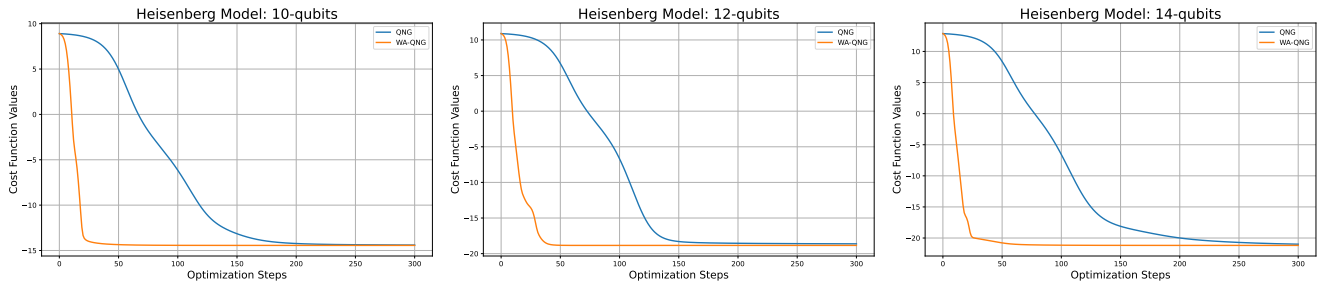


FIG. 6. The learning curves of the two methods for Heisenberg model of 10, 12, 14 qubits.

system indeed improves optimization performance. The second is the Hilbert-Schmidt metric tensor for each subsystem provides a better representation of parameter sensitivity within subsystems compared to using the quantum Fisher information matrix of the entire system. The experimental results are consistent with the theoretical analysis.

In Section IV and Section III C, we mention that WA-QNG has a stronger theoretical explanation from both its approximation to quantum Fisher information matrix and its connection with Gauss-Newton method when each subsystem state is close to being pure and does not change significantly with parameters. However, this assumption is not necessary for WA-QNG to perform better than standard QNG. In the experiments, we observe that WA-QNG still outperforms standard QNG, even when the final target is an entanglement state where each subsystem is mixed.

Since the focus of this paper is to introduce the novelty of WA-QNG itself, we track the exact expectation values and metric tensors of the quantum circuit. In practical applications, these quantities can only be estimated through finite shots, which introduces shot noise. Additionally, we assume that the circuit is noise-free, which is not the case in real-world implementations. Investigating the effects of shot noise and circuit noise on WA-QNG is left as a potential direction for future work.

This work primarily focuses on optimization for the

quantum variational eigensolver. However, since QNG can also be applied to optimize other variational quantum algorithms such as the variational quantum classifier in the field of machine learning, we believe WA-QNG is expected to be extendable to these tasks similarly. Evaluating the performance of WA-QNG in these applications is beyond the scope of this work but remains a promising direction for future research.

In conclusion, WA-QNG offers a promising and efficient optimization method for variational quantum eigensolvers. By accounting for the weights of each subsystem that contributes to the output, WA-QNG presents a potential research direction for optimization in variational quantum algorithms.

## VII. ACKNOWLEDGMENT

All authors acknowledge the support from the Dutch National Growth Fund (NGF), as part of the Quantum Delta NL programme. V.D. acknowledges support from the Dutch Research Council (NWO/OCW), as part of the Quantum Software Consortium programme (project number 024.003.03). This project was also co-funded by the European Union (ERC CoG, BeMAIQuantum, 101124342).

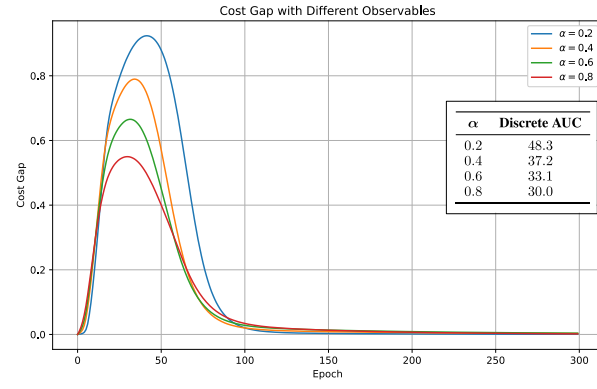


FIG. 7. The cost function value gap curves and corresponding discrete AUC between WA-QNG and QNG under different values of  $\alpha$  for the Hamiltonian  $H = Z_1 Z_2 + Z_2 Z_3 + \alpha X_1 + (3 - 2\alpha) X_2 + \alpha X_3$ . A smaller  $\alpha$  increases the weight of the subsystem on the second qubit in the output, leading to a scenario where WA-QNG should outperform QNG more significantly. This figure indicates that the theoretical analysis aligns with the experimental results that WA-QNG indeed achieves greater performance improvement over QNG as  $\alpha$  gradually decreases.

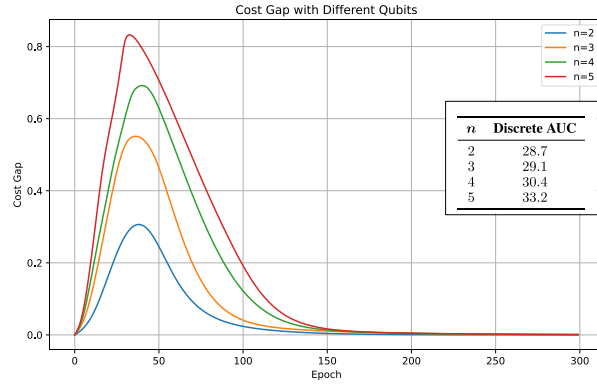


FIG. 8. The cost function value gap curves and corresponding discrete AUC between WA-QNG and QNG under different values of  $n$  for the Hamiltonian  $H = \sum_{i=1}^{n-1} Z_i Z_{i+1} + \sum_{i=1}^n X_i$ . A larger  $n$  increases the difference in parameter sensitivity of each subsystem compared to that of the entire system, leading to a scenario where WA-QNG should outperform QNG more significantly. This figure shows that the theoretical analysis aligns with the experimental results, indicating that WA-QNG achieves greater performance improvement over QNG as  $n$  increases with a fixed locality factor  $k$ .

## APPENDIX

## Appendix A: QNG as a special case of WA-QNG

When any term  $H_m$  in the Hamiltonian is related to the entire quantum system, each corresponding subsystem  $\rho_m$  also becomes the whole system  $\rho_\theta$ . In this scenario, each  $T_m$  no longer depends on the index  $m$ , causing the terms  $\sum_m h_m^2$  in the weighted summation to cancel out with that in the prefactor. As a consequence, the matrix  $W$  exactly reduces to the Hilbert-Schmidt metric tensor of the whole quantum system  $\rho_\theta$  with a constant factor 2, where the  $i$ -th row and  $j$ -th column element of the matrix  $W$  is as follows:

$$W_{ij} = 2\text{tr}(\partial_i \rho_\theta \partial_j \rho_\theta) \quad (\text{A1})$$

Now we prove the matrix  $W$  is equal to the quantum Fisher information matrix  $F$ . The variational state  $\rho_\theta$  on the whole system is a pure state, so we can write the state  $\rho_\theta$  as  $\rho_\theta = |\phi\rangle\langle\phi|$ . So we only have to prove the right side of Eq. (A1) is equal to that of Eq. (6):

$$\begin{aligned} W_{ij} &= 2\text{tr}(\partial_i \rho \partial_j \rho) \\ &= 2\text{tr}(\partial_i (|\phi\rangle\langle\phi|) \partial_j (|\phi\rangle\langle\phi|)) \\ &= 2\text{tr}((|\partial_i \phi\rangle\langle\phi| + |\phi\rangle\langle\partial_i \phi|)(|\partial_j \phi\rangle\langle\phi| + |\phi\rangle\langle\partial_j \phi|)) \\ &= 2\text{tr}(|\partial_i \phi\rangle\langle\phi| \partial_j \phi \langle\phi| + |\partial_i \phi\rangle\langle\partial_j \phi| + |\phi\rangle\langle\partial_i \phi| \partial_j \phi \langle\phi| + |\phi\rangle\langle\partial_j \phi|) \\ &= 2\langle\phi|\partial_j \phi\rangle\langle\phi|\partial_i \phi\rangle + 2\langle\partial_i \phi|\phi\rangle\langle\partial_j \phi|\phi\rangle + 2\langle\partial_j \phi|\partial_i \phi\rangle + 2\langle\partial_i \phi|\partial_j \phi\rangle \\ &= 2\langle\partial_j \phi|\partial_i \phi\rangle + 2\langle\partial_i \phi|\partial_j \phi\rangle - 2\langle\phi|\partial_j \phi\rangle\langle\partial_i \phi|\phi\rangle - 2\langle\phi|\partial_i \phi\rangle\langle\partial_j \phi|\phi\rangle \\ &= 4\text{Re}(\langle\partial_i \phi|\partial_j \phi\rangle - \langle\partial_i \phi|\phi\rangle\langle\phi|\partial_j \phi\rangle) \\ &= F_{ij} \end{aligned} \quad (\text{A2})$$

## Appendix B: Estimate Hilbert-Schmidt Metric Tensor via Classical Shadows

In this section, we demonstrate that the Hilbert-Schmidt metric tensor  $T$ <sup>3</sup> used in WA-QNG can be efficiently estimated by classical shadow and bound the shots required to obtain the element  $T_{ij}$ . To avoid confusion in the derivation, we will use calligraphic font  $\mathcal{T}$  to represent the Hilbert-Schmidt metric tensor in the following section.

## 1. Parameter-Shift Rule

First, the parameter-shift rule can be applied to compute each element of the matrix  $\mathcal{T}$ :

$$\begin{aligned} \mathcal{T}_{ij} &= 2\text{tr}(\partial_i \rho_\theta \partial_j \rho_\theta) \\ &= \frac{1}{2}\text{tr}\left((\rho_{\theta+\frac{\pi}{2}e_i} - \rho_{\theta-\frac{\pi}{2}e_i})(\rho_{\theta+\frac{\pi}{2}e_j} - \rho_{\theta-\frac{\pi}{2}e_j})\right) \\ &= \frac{1}{2}\left(\text{tr}(\rho_{\theta+\frac{\pi}{2}e_i}\rho_{\theta+\frac{\pi}{2}e_j}) - \text{tr}(\rho_{\theta+\frac{\pi}{2}e_i}\rho_{\theta-\frac{\pi}{2}e_j}) - \text{tr}(\rho_{\theta-\frac{\pi}{2}e_i}\rho_{\theta+\frac{\pi}{2}e_j}) + \text{tr}(\rho_{\theta-\frac{\pi}{2}e_i}\rho_{\theta-\frac{\pi}{2}e_j})\right) \end{aligned} \quad (\text{B1})$$

where  $e_i$  represents the unit vector with the  $i$ -th element set to one and all other elements set to zero. To estimate  $\mathcal{T}_{ij}$ , we only need to estimate the four terms in Eq. (B1) respectively. To estimate the entire matrix  $\mathcal{T}$ , we can estimate each element individually, meaning the total cost scales quadratically with the number of parameters. Thus, if we can bound the cost of estimating the term like  $\text{tr}(\rho\sigma)$ , we can also bound the total cost. In our case, where the Hamiltonian is  $k$ -local, we show the cost of estimating such term  $\text{tr}(\rho\sigma)$  via classical shadow is exponential to the subsystem size  $k$  rather than the size of the whole system  $n$ .

---

<sup>3</sup> Here for notation simplify, we omit the subscript for each  $T_m$  in the definition of the matrix  $W$  in Section III B

## 2. Classical Shadow

The classical shadow technique constructs a series of unbiased estimators  $\hat{\rho}^{(t)}$  ( $1 \leq t \leq T$ , where  $T$  is the total number of the classical shadows constructed) for a state  $\rho$ , with the property that  $\mathbb{E}[\hat{\rho}^{(t)}] = \rho$ . Each  $\hat{\rho}^{(t)}$  is represented as:

$$\hat{\rho}^{(t)} = \bigotimes_{i=1}^n (3U_i^\dagger |\hat{b}_i\rangle \langle \hat{b}_i| U_i - \mathbb{I}) \quad (\text{B2})$$

where  $n$  is the system size,  $b$  is a binary string obtained by measurements, and  $b_i$  represents the  $i$ -th bit of  $b$  (either 0 or 1).  $U$  denotes the corresponding random Pauli gate applied to the  $i$ -th qubit. For more details on the data acquisition process in the classical shadow technique, please refer to [18] and [32]. Two important properties of each estimator  $\hat{\rho}^{(t)}$  are as follows:

$$\mathbb{E}[\text{tr}(\hat{\rho}^{(t)} O)] = \text{tr}(\rho O) \quad (\text{B3})$$

$$\text{Var}[\text{tr}(\hat{\rho}^{(t)} O)] \leq 2^{w(O)} \text{tr}(O^2) \quad (\text{B4})$$

where  $w(O)$  represents the number of qubits on which the observable  $O$  acts nontrivially. For the details of derivation of Eq. (B3) and Eq. (B4), please refer to the paper [33].

To reduce error, an empirical average is taken over all samples to construct the estimator  $\hat{\rho}$ :

$$\hat{\rho} = \frac{1}{T} \sum_i^T \hat{\rho}^{(t)} \quad (\text{B5})$$

From Eq. (B3) and Eq. (B4), the following properties of the estimator  $\hat{\rho}$  can be derived:

$$\mathbb{E}[\text{tr}(\hat{\rho} O)] = \text{tr}(\rho O) \quad (\text{B6})$$

$$\text{Var}[\text{tr}(\hat{\rho} O)] \leq \frac{2^{w(O)} \text{tr}(O^2)}{T} \quad (\text{B7})$$

## 3. Construct Estimator for Hilbert-Schmidt Metric Tensor

As discussed in Appendix B1, estimating the Hilbert-Schmidt metric tensor via the classical shadow technique requires constructing an estimator for terms like  $\text{tr}(\rho\sigma)$ . Similar to the estimator used for estimating purity in [18] and [33], the following estimator can be constructed for the term like  $\text{tr}(\rho\sigma)$ . For simplicity, we denote  $p = \text{tr}(\rho\sigma)$ , then the corresponding estimator  $\hat{p}$  is:

$$\hat{p} = \frac{1}{T^2} \sum_{ij} \text{tr}(\hat{\rho}^{(i)} \hat{\sigma}^{(j)}) \quad (\text{B8})$$

where each  $\hat{\rho}^{(i)}$  and  $\hat{\sigma}^{(j)}$  ( $1 \leq i, j \leq T$ ) is obtained using the classical shadow technique as described in Eq. (B2). Because  $\hat{\rho}^{(i)}$  and  $\hat{\sigma}^{(j)}$  are independent, we have:

$$\begin{aligned} \mathbb{E}[\hat{p}] &= \mathbb{E}\left[\frac{1}{T^2} \sum_{ij} \text{tr}(\hat{\rho}^{(i)} \hat{\sigma}^{(j)})\right] \\ &= \frac{1}{T^2} \sum_{ij} \mathbb{E}[\text{tr}(\hat{\rho}^{(i)} \hat{\sigma}^{(j)})] \\ &= \frac{1}{T^2} \sum_{ij} \text{tr}(\mathbb{E}[\hat{\rho}^{(i)}] \mathbb{E}[\hat{\sigma}^{(j)}]) \\ &= \text{tr}(\rho\sigma) \\ &= p \end{aligned} \quad (\text{B9})$$

Hence, the estimator  $\hat{p}$  is also an unbiased estimator for  $p$ . To bound the computational cost, we also need to bound the variance of the estimator  $\hat{p}$ .

#### 4. Bounding Variance

According to the definition of the variance of a random variable, we have:  $\hat{p}$ .

$$\begin{aligned} \text{Var}[\hat{p}] &= \text{E}[(\hat{p} - p)^2] \\ &= \text{E} \left[ \left( \frac{1}{T^2} \sum_{ij} (\text{tr}(\hat{\rho}^{(i)} \hat{\sigma}^{(j)}) - \text{tr}(\rho\sigma)) \right)^2 \right] \\ &= \frac{1}{T^4} \sum_{ij} \sum_{kl} \text{E} \left[ (\text{tr}(\hat{\rho}^{(i)} \hat{\sigma}^{(k)}) - \text{tr}(\rho\sigma)) (\text{tr}(\hat{\rho}^{(j)} \hat{\sigma}^{(l)}) - \text{tr}(\rho\sigma)) \right] \end{aligned} \quad (\text{B10})$$

The summation in Eq. (B10) can be divided into the following three cases. Suppose the density operator  $\rho$  and  $\sigma$  are systems of  $n$ -qubit.

1. When  $i \neq k$  and  $j \neq l$ : There are  $T^2(T-1)^2$  terms. For each term, we have:

$$\begin{aligned} &\text{E} \left[ (\text{tr}(\hat{\rho}^{(i)} \hat{\sigma}^{(j)}) - \text{tr}(\rho\sigma)) (\text{tr}(\hat{\rho}^{(k)} \hat{\sigma}^{(l)}) - \text{tr}(\rho\sigma)) \right] \\ &= (\text{E}[\text{tr}(\hat{\rho}^{(i)} \hat{\sigma}^{(j)})] - \text{tr}(\rho\sigma)) (\text{E}[\text{tr}(\hat{\rho}^{(k)} \hat{\sigma}^{(l)})] - \text{tr}(\rho\sigma)) \\ &= 0 \end{aligned} \quad (\text{B11})$$

2. When  $i = k$  but  $j \neq l$ , or  $j = l$  but  $i \neq k$ : There are  $2T^2(T-1)$  terms. Without loss of generality, we take the case where  $i = k$  but  $j \neq l$  as an example. The calculation in another case is the same. For each term, we have:

$$\begin{aligned} &\text{E} \left[ (\text{tr}(\hat{\rho}^{(i)} \hat{\sigma}^{(j)}) - \text{tr}(\rho\sigma)) (\text{tr}(\hat{\rho}^{(i)} \hat{\sigma}^{(l)}) - \text{tr}(\rho\sigma)) \right] \\ &= \text{E} [\text{tr}(\hat{\rho}^{(i)} \hat{\sigma}^{(j)}) \text{tr}(\hat{\rho}^{(i)} \hat{\sigma}^{(l)})] - \text{tr}^2(\rho\sigma) \\ &= \text{E} [\text{tr}(\hat{\rho}^{(i) \otimes 2} \hat{\sigma}^{(j)} \otimes \hat{\sigma}^{(l)})] - \text{tr}^2(\rho\sigma) \\ &= \text{E} [\text{tr}^2(\hat{\rho}^{(i)} \sigma)] - \text{tr}^2(\rho\sigma) \\ &= \text{Var}[\text{tr}(\hat{\rho}^{(i)} \sigma)] \\ &\leq 2^{w(\sigma)} \text{tr}(\sigma^2) \\ &\leq 2^n \end{aligned} \quad (\text{B12})$$

The third equality in Eq. (B12) relies on the property that, when the unbiased estimators  $\hat{\rho}$  and  $\hat{\sigma}$  are independent, then  $\text{E}[\hat{\rho} \otimes \hat{\sigma}] = \rho \otimes \sigma$ . The details of this property can be found in [33]. The first inequality is from Eq. (B4).

3. When  $i = k$  and  $j = l$ : There are  $T^2$  terms. For each term, we have:

$$\begin{aligned} &\text{E} \left[ (\text{tr}(\hat{\rho}^{(i)} \hat{\sigma}^{(j)}) - \text{tr}(\rho\sigma)) (\text{tr}(\hat{\rho}^{(i)} \hat{\sigma}^{(j)}) - \text{tr}(\rho\sigma)) \right] \\ &= \text{E} [\text{tr}^2(\hat{\rho}^{(i)} \hat{\sigma}^{(j)})] - \text{tr}^2(\rho\sigma) \\ &= \text{Var}[\text{tr}(\hat{\rho}^{(i)} \hat{\sigma}^{(j)})] \\ &= \text{Var}[\text{tr}(S \hat{\rho}^{(i)} \otimes \hat{\sigma}^{(j)})] \\ &\leq 2^{w(S)} \text{tr}(S^2) \\ &= 2^{4n} \end{aligned} \quad (\text{B13})$$

The third equality follows from the property  $\text{tr}(S \rho \otimes \sigma) = \text{tr}(\rho\sigma)$ , where  $S \in \mathbb{C}^{2^{2n} \times 2^{2n}}$  is the *SWAP* operator. The details of this property can be found in [34]. The inequality arises from Eq. (B4). The last equality holds because  $S$  acts on  $2^{2n}$  qubits and satisfies  $S^2 = I$ .

Hence, the final result of Eq. (B10) shall be upper bounded by:

$$\begin{aligned}\text{Var}[\hat{p}] &= \frac{1}{T^4} \sum_{ij} \sum_{kl} \mathbb{E} \left[ (\text{tr}(\hat{\rho}^{(i)} \hat{\sigma}^{(k)}) - \text{tr}(\rho\sigma)) (\text{tr}(\hat{\rho}^{(j)} \hat{\sigma}^{(l)}) - \text{tr}(\rho\sigma)) \right] \\ &\leq \frac{1}{T^4} (2T^2(T-1)2^n + T^2 2^{4n}) \\ &\leq \frac{2^{n+1}}{T} + \frac{2^{4n}}{T^2}\end{aligned}\tag{B14}$$

## 5. Bounding Shots

Using the bound of variance Eq. (B14), we can derive the upper bound of total shots required in the estimation for the term like  $\text{tr}(\rho\sigma)$ . Following the assumption in the reference paper [32] that, the  $T$  can be very large where the expression of Eq. (B14) is dominated by the first term. Following Chebyshev's inequality:

$$\Pr[|\hat{p} - p| \geq \epsilon] \lesssim \frac{2^{n+1}}{T\epsilon^2}\tag{B15}$$

Then, a measurement budget that scales as

$$T \geq \frac{2^{n+1}}{\epsilon^2 \delta}\tag{B16}$$

with probability  $1 - \delta$  suffice to control the estimation error below  $\epsilon$ . Hence, the lower bound of shots required to estimate a term like  $\text{tr}(\rho\sigma)$  is  $\Omega(2^{n+1})$ , where  $n$  is the system size of the quantum density operator  $\rho$  and  $\sigma$ .

In our case, there are four terms like  $\text{tr}(\rho\sigma)$  in the Eq. (B1) required to estimate for the element  $\mathcal{T}_{ij}$ , and each term is only  $k$ -local. Hence the cost of shots required to estimate each element  $\mathcal{T}_{ij}$  is  $\Omega(4 \cdot 2^{k+1})$ , which is exponential to the subsystem size  $k$  instead of the entire system size  $n$ .

## Appendix C: Approximate Quantum Fisher Information via Hilbert-Schmidt Metric Tensor

In this section, we provide a simple proof that the Hilbert-Schmidt metric tensor serves as an approximation to the quantum Fisher information matrix  $F$  when the state  $\rho$  is close to being pure and does not change significantly with parameters. Moreover, this approximation becomes exact when  $\rho$  is pure.

For a state  $\rho = \sum_{k=1}^n r_k |r_k\rangle \langle r_k|$ , suppose the dominant eigenvector [24, 25] is  $|r_d\rangle$  with eigenvalue  $r_d$ . When state  $\rho$  is close to being pure, the dominant eigenvalue satisfies  $r_d \approx 1$ , while all other eigenvalues satisfy  $r_k \approx 0$ . For the state  $\rho$ , we show its Hilbert-Schmidt metric tensor can be computed and simplified as:

$$\begin{aligned}\text{tr}(\partial_i \rho \partial_j \rho) &= \sum_k \frac{\partial r_k}{\partial \theta_i} \cdot \frac{\partial r_j}{\partial \theta_j} + \sum_k r_k^2 \frac{F_k}{2} - \sum_{kl, k \neq l} r_k r_l \cdot 2 \text{Re}[\langle \partial_i r_k | r_l \rangle \langle r_k | \partial_j r_l \rangle] \\ &\approx \frac{r_d^2}{2} (F_d)_{ij} \\ &\approx \frac{1}{2} F_{ij}\end{aligned}\tag{C1}$$

where  $(F_d)_{ij}$  represents the  $(i, j)$ -th element of the quantum Fisher information matrix of the dominant state. The derivation of the first equation will be explained in detail in the following discussion. When the state  $\rho$  is close to being pure, the other eigenvalues are higher-order infinitesimals compared to the dominant eigenvalues. Consequently, the second and third terms in the first equation can be approximated as  $\frac{r_d^2}{2} (F_d)_{ij}$ . If the state does not change drastically with respect to the parameters, the first term will also be small. In practical applications, this can be achieved by initializing the variational quantum circuit with low entanglement and setting the learning rate to a small value. Moreover, because  $r_d \approx 1$  and the state  $|r_d\rangle$  dominates  $\rho$ , we can obtain  $\frac{r_d^2}{2} (F_d)_{ij} \approx \frac{1}{2} F_{ij}$ .

Now, we provide a brief derivation of the first equation. For simplicity of notation, we denote the three terms in  $\partial_i \rho = \sum_k \partial_i r_k |r_k\rangle \langle r_k| + \sum_k r_k |\partial_i r_k\rangle \langle r_k| + \sum_k r_k |r_k\rangle \langle \partial_i r_k|$  as  $A_i$ ,  $B_i$ , and  $C_i$  respectively. Similarly, for  $\partial_j \rho$  we can also denote  $A_j$ ,  $B_j$  and  $C_j$  for the three terms analogously. Hence, we can express:

$$\begin{aligned}\text{tr}(\partial_i \rho \partial_j \rho) & \\ &= \text{tr}(A_i A_j) + \text{tr}(A_i B_j) + \text{tr}(A_i C_j) + \text{tr}(B_i A_j) + \text{tr}(B_i B_j) + \text{tr}(B_i C_j) + \text{tr}(C_i A_j) + \text{tr}(C_i B_j) + \text{tr}(C_i C_j)\end{aligned}\tag{C2}$$

We can compute these terms separately.

1.  $\text{tr}(A_i A_j)$ :

$$\begin{aligned}\text{tr}(A_i A_j) &= \text{tr}\left(\sum_k \frac{\partial r_k}{\partial \theta_i} \frac{\partial r_k}{\partial \theta_j} |r_k\rangle \langle r_k|\right) \\ &= \sum_k \frac{\partial r_k}{\partial \theta_i} \frac{\partial r_k}{\partial \theta_j}\end{aligned}\quad (\text{C3})$$

2.  $\text{tr}(A_i B_j)$  and  $\text{tr}(A_i C_j)$ :

$$\begin{aligned}\text{tr}(A_i C_j) + \text{tr}(A_i B_j) &= \sum_k \frac{\partial r_k}{\partial \theta_i} r_k \langle \partial_j r_k | r_k \rangle + \sum_k \frac{\partial r_k}{\partial \theta_i} r_k \langle r_k | \partial_j r_k \rangle \\ &= 0\end{aligned}\quad (\text{C4})$$

3.  $\text{tr}(B_i C_j)$  and  $\text{tr}(C_i B_j)$ :

$$\begin{aligned}\text{tr}(B_i C_j) + \text{tr}(C_i B_j) &= \sum_k r_k^2 \langle \partial_j r_k | \partial_i r_k \rangle + \sum_k r_k^2 \langle \partial_i r_k | \partial_j r_k \rangle \\ &= \sum_k 2r_k^2 \text{Re}[\langle \partial_i r_k | \partial_j r_k \rangle]\end{aligned}\quad (\text{C5})$$

4.  $\text{tr}(B_i B_j)$  and  $\text{tr}(C_i C_j)$ :

$$\begin{aligned}\text{tr}(B_i B_j) + \text{tr}(C_i C_j) &= \sum_{kl} r_k r_l (\langle r_k | \partial_j r_l \rangle \langle r_l | \partial_i r_k \rangle + \langle \partial_i r_k | r_l \rangle \langle \partial_i r_k | r_l \rangle \langle \partial_j r_l | r_k \rangle) \\ &= -\sum_k r_k^2 \cdot 2 \text{Re}[\langle \partial_i r_k | r_k \rangle \langle r_k | \partial_j r_k \rangle] - \sum_{kl, k \neq l} r_k r_l \cdot 2 \text{Re}[\langle \partial_i r_k | r_l \rangle \langle r_k | \partial_j r_l \rangle]\end{aligned}\quad (\text{C6})$$

5.  $\text{tr}(C_i A_j)$  and  $\text{tr}(B_i A_j)$ :

$$\begin{aligned}\text{tr}(C_i A_j) + \text{tr}(B_i A_j) &= r_k^2 \langle r_k | \partial_i r_k \rangle + r_k^2 \langle \partial_i r_k | r_k \rangle \\ &= 0\end{aligned}\quad (\text{C7})$$

By combining these results, we obtain the first equation in Eq. (C1).

#### Appendix D: Deriving WA-QNG Optimization Step from Geometric Interpretation

According to the Lagrange multiplier method, the constrained optimization problem in Eq. (12) can be formulated as:

$$d^* = \underset{d}{\text{argmin}} f(\theta + d) + \lambda \left( \frac{2}{\sum_m h_m^2} \sum_m h_m^2 \|\rho_m(\theta + d) - \rho_m(\theta)\|_2^2 - \epsilon \right) \quad (\text{D1})$$

For the trace 2-norm term, applying the first-order Taylor expansion to  $\rho_m(\theta + d)$ , we obtain:

$$\begin{aligned}\|\rho_m(\theta + d) - \rho_m(\theta)\|_2^2 &\approx \|\rho_m(\theta) + \sum_i \partial_i \rho_m(\theta) d_i - \rho_m(\theta)\|_2^2 \\ &= \left\| \sum_i \partial_i \rho_m(\theta) d_i \right\|_2^2 \\ &= \text{tr} \left( \sum_i \sum_j \partial_i \rho_m \partial_j \rho_m d_i d_j \right) \\ &= \sum_i \sum_j \text{tr}(\partial_i \rho_m \partial_j \rho_m) d_i d_j\end{aligned}\quad (\text{D2})$$

Substituting Eq. (D2) into Eq. (D1) and applying the first-order Taylor expansion to  $f(\theta + d)$ , we obtain:

$$\begin{aligned}
d^* &\approx \underset{d}{\operatorname{argmin}} f(\theta) + \nabla f(\theta)^T d + \frac{2\lambda}{\sum_m h_m^2} \sum_m h_m^2 \sum_i \sum_j \operatorname{tr}(\partial_i \rho_m \partial_j \rho_m) d_i d_j - \lambda \epsilon \\
&= \underset{d}{\operatorname{argmin}} f(\theta) + \nabla f(\theta)^T d + \sum_i \sum_j \left( \frac{2\lambda}{\sum_m h_m^2} \sum_m h_m^2 \operatorname{tr}(\partial_i \rho_m \partial_j \rho_m) \right) d_i d_j - \lambda \epsilon \\
&= \underset{d}{\operatorname{argmin}} f(\theta) + \nabla f(\theta)^T d + \lambda d^T W d - \lambda \epsilon
\end{aligned} \tag{D3}$$

where the matrix  $W$  is exactly the same matrix defined in WA-QNG in Eq. (7). Since we are computing the minimum, Eq. (D3) should satisfy the Karush–Kuhn–Tucker (KKT) conditions [35]. Here, it simply means that the derivative of the right side with respect to  $d$  should be zero:

$$\begin{aligned}
0 &= \nabla f(\theta) + 2\lambda W d \\
d &= -\frac{1}{2\lambda} W^+ \nabla f(\theta)
\end{aligned} \tag{D4}$$

Eq. (D4) indicates the optimal update direction in WA-QNG. Since the Lagrange multiplier  $\lambda$  can be absorbed into the learning rate, the above formula can be exactly transformed into the update formula of WA-QNG, as given in Eq. (7).

### Appendix E: Relation with Gauss-Newton Method Supplement

Here we verify the relation  $W = 2J_r^T J_r$ . The  $(i, j)$ -th element of the Jacobian  $J_r$  is:

$$\begin{aligned}
(J_r)_{ij} &= \frac{h_i}{\sqrt{\sum_m h_m^2}} \frac{\partial(\operatorname{vec}(\rho_i) - \operatorname{vec}(\tilde{H}_i))}{\partial \theta_j} \\
&= \frac{h_i}{\sqrt{\sum_m h_m^2}} \frac{\partial \operatorname{vec}(\rho_i)}{\partial \theta_j}
\end{aligned} \tag{E1}$$

Hence, the  $(i, j)$ -th element of  $J_r^T J_r$  should be:

$$\begin{aligned}
(J_r^T J_r)_{ij} &= \sum_k (J_r^T)_{ik} (J_r)_{kj} \\
&= \sum_k \frac{h_k}{\sqrt{\sum_m h_m^2}} \frac{h_k}{\sqrt{\sum_m h_m^2}} \left( \frac{\partial \operatorname{vec}(\rho_k)}{\partial \theta_i} \cdot \frac{\partial \operatorname{vec}(\rho_k)}{\partial \theta_j} \right) \\
&= \frac{1}{\sum_m h_m^2} \sum_k h_k^2 \operatorname{tr}(\partial_i \rho_k \partial_j \rho_k) \\
&= \frac{1}{\sum_m h_m^2} \sum_m h_m^2 (T_m)_{ij} \\
&= \frac{1}{2} W_{ij}
\end{aligned} \tag{E2}$$

Hence, we have proved the relation  $W = 2J_r^T J_r$ .

- 
- [1] J. Preskill, Quantum computing in the nisq era and beyond, *Quantum* **2**, 79 (2018).  
[2] P. W. Shor, Polynomial-time algorithms for prime factorization and discrete logarithms on a quantum computer, *SIAM review* **41**, 303 (1999).  
[3] L. K. Grover, A fast quantum mechanical algorithm for database search, in *Proceedings of the twenty-eighth annual ACM symposium on Theory of computing* (1996) pp. 212–219.  
[4] K. Bharti, A. Cervera-Lierta, T. H. Kyaw, T. Haug, S. Alperin-Lea, A. Anand, M. Degroote, H. Heimonen, J. S. Kottmann, T. Menke, *et al.*, Noisy intermediate-



- scale quantum algorithms, *Reviews of Modern Physics* **94**, 015004 (2022).
- [5] N. Moll, P. Barkoutsos, L. S. Bishop, J. M. Chow, A. Cross, D. J. Egger, S. Filipp, A. Fuhrer, J. M. Gambetta, M. Ganzhorn, *et al.*, Quantum optimization using variational algorithms on near-term quantum devices, *Quantum Science and Technology* **3**, 030503 (2018).
- [6] A. Aspuru-Guzik, A. D. Dutoi, P. J. Love, and M. Head-Gordon, Simulated quantum computation of molecular energies, *Science* **309**, 1704 (2005).
- [7] A. Peruzzo, J. McClean, P. Shadbolt, M.-H. Yung, X.-Q. Zhou, P. J. Love, A. Aspuru-Guzik, and J. L. O’Brien, A variational eigenvalue solver on a photonic quantum processor, *Nature communications* **5**, 4213 (2014).
- [8] E. Farhi, J. Goldstone, and S. Gutmann, A quantum approximate optimization algorithm, arXiv preprint arXiv:1411.4028 (2014).
- [9] C. Grange, M. Poss, and E. Bourreau, An introduction to variational quantum algorithms for combinatorial optimization problems, *4OR* **21**, 363 (2023).
- [10] V. Havlíček, A. D. Córcoles, K. Temme, A. W. Harrow, A. Kandala, J. M. Chow, and J. M. Gambetta, Supervised learning with quantum-enhanced feature spaces, *Nature* **567**, 209 (2019).
- [11] S. Jerbi, L. J. Fiderer, H. Poulsen Nautrup, J. M. Kübler, H. J. Briegel, and V. Dunjko, Quantum machine learning beyond kernel methods, *Nature Communications* **14**, 1 (2023).
- [12] H. Robbins and S. Monro, A stochastic approximation method, *The annals of mathematical statistics* , 400 (1951).
- [13] P. K. Diederik, Adam: A method for stochastic optimization, (No Title) (2014).
- [14] J. Stokes, J. Izaac, N. Killoran, and G. Carleo, Quantum natural gradient, *Quantum* **4**, 269 (2020).
- [15] S.-I. Amari, Natural gradient works efficiently in learning, *Neural computation* **10**, 251 (1998).
- [16] J. Martens, New insights and perspectives on the natural gradient method, *Journal of Machine Learning Research* **21**, 1 (2020).
- [17] J. Liu, H. Yuan, X.-M. Lu, and X. Wang, Quantum fisher information matrix and multiparameter estimation, *Journal of Physics A: Mathematical and Theoretical* **53**, 023001 (2020).
- [18] H.-Y. Huang, R. Kueng, and J. Preskill, Predicting many properties of a quantum system from very few measurements, *Nature Physics* **16**, 1050 (2020).
- [19] K. Mitarai, M. Negoro, M. Kitagawa, and K. Fujii, Quantum circuit learning, *Physical Review A* **98**, 032309 (2018).
- [20] M. Schuld, V. Bergholm, C. Gogolin, J. Izaac, and N. Killoran, Evaluating analytic gradients on quantum hardware, *Physical Review A* **99**, 032331 (2019).
- [21] Y. Ollivier, L. Arnold, A. Auger, and N. Hansen, Information-geometric optimization algorithms: A unifying picture via invariance principles, *Journal of Machine Learning Research* **18**, 1 (2017).
- [22] Y. Yao, P. Cussenot, R. A. Wolf, and F. Miatto, Complex natural gradient optimization for optical quantum circuit design, *Phys. Rev. A* **105**, 052402 (2022).
- [23] N. Yamamoto, On the natural gradient for variational quantum eigensolver, arXiv preprint arXiv:1909.05074 (2019).
- [24] B. Koczor and S. C. Benjamin, Quantum natural gradient generalized to noisy and nonunitary circuits, *Physical Review A* **106**, 062416 (2022).
- [25] B. Koczor and S. C. Benjamin, Quantum analytic descent, *Physical Review Research* **4**, 023017 (2022).
- [26] J. L. Beckey, M. Cerezo, A. Sone, and P. J. Coles, Variational quantum algorithm for estimating the quantum fisher information, *Physical Review Research* **4**, 013083 (2022).
- [27] J. M. Lee, *Introduction to Riemannian manifolds*, Vol. 2 (Springer, 2018).
- [28] J. Gacon, C. Zoufal, G. Carleo, and S. Woerner, Simultaneous perturbation stochastic approximation of the quantum fisher information, *Quantum* **5**, 567 (2021).
- [29] J. Nocedal and S. J. Wright, *Numerical optimization* (Springer, 1999).
- [30] M. Larocca, S. Thanasilp, S. Wang, K. Sharma, J. Biamonte, P. J. Coles, L. Cincio, J. R. McClean, Z. Holmes, and M. Cerezo, A review of barren plateaus in variational quantum computing, arXiv preprint arXiv:2405.00781 (2024).
- [31] K. Zhang, L. Liu, M.-H. Hsieh, and D. Tao, Escaping from the barren plateau via gaussian initializations in deep variational quantum circuits, *Advances in Neural Information Processing Systems* **35**, 18612 (2022).
- [32] S. H. Sack, R. A. Medina, A. A. Michailidis, R. Kueng, and M. Serbyn, Avoiding barren plateaus using classical shadows, *PRX Quantum* **3**, 020365 (2022).
- [33] A. Neven, J. Carrasco, V. Vitale, C. Kokail, A. Elben, M. Dalmonte, P. Calabrese, P. Zoller, B. Vermersch, R. Kueng, *et al.*, Symmetry-resolved entanglement detection using partial transpose moments, *npj Quantum Information* **7**, 152 (2021).
- [34] A. A. Mele, Introduction to haar measure tools in quantum information: A beginner’s tutorial, *Quantum* **8**, 1340 (2024).
- [35] H. Kuhn and A. Tucker, Proceedings of 2nd berkeley symposium, in *Proceedings of 2nd Berkeley Symposium* (1951) pp. 481–492.